Am J Cancer Res 2020;10(9):2752-2767
www.ajcr.us /ISSN:2156-6976/ajcr0116621

Original Article

The role of Nrf2/PIWIL2/purine metabolism axis in controlling radiation-induced lung fibrosis

Guan-Lian Zou[1,2*], Xiao-Ran Zhang[1*], Yan-Li Ma[1*], Qing Lu[3,4], Ren Zhao[3,4], Yong-Zhao Zhu[5], Yan-Yang Wang[3,4]

[1]Graduate School, Ningxia Medical University, Yinchuan 750004, Ningxia, China; [2]Department of Radiation Oncology II, Zhongshan People's Hospital, Zhongshan 528403, Guangdong, China; [3]Department of Radiation Oncology, General Hospital of Ningxia Medical University, Yinchuan 750004, Ningxia, China; [4]Cancer Institute, Ningxia Medical University, Yinchuan 750004, Ningxia, China; [5]Surgical Laboratory, General Hospital of Ningxia Medical University, Yinchuan 750004, Ningxia, China. [*]Equal contributors.

Received June 19, 2020; Accepted August 14, 2020; Epub September 1, 2020; Published September 15, 2020

Abstract: NF-E2-related factor 2 (Nrf2) is a key transcription factor recently implicated in the control of radiation-induced lung fibrosis (RILF). However, the molecular mechanism of Nrf2 in the pathogenesis of RILF is still unclear. The purpose of this study was to evaluate the regulatory effect and mechanism of Nrf2 in the pathogenesis of RILF. The effects of different Nrf2 expression levels on RILF were explored in vitro and in vivo. The RILF model of Nrf2 knockout mice was established for in vivo study. In the study of the mechanism of action, ChIP-seq assay and metabolomics analysis were performed. The discovered mechanism of Nrf2-mediated RILF alleviation was further validated in vitro and in vivo. We found that overexpression of Nrf2 significantly alleviated the fibrosis caused by irradiation in vivo and in vitro. Conversely, Nrf2 silencing strongly aggravated the development of RILF. Mechanistically, Nrf2 signaling increased the expression of piwi-like RNA-mediated gene silencing 2 (PIWIL2), leading to the alteration of purine metabolism and contributing to the relief of RILF. These results suggest that Nrf2 promotes the attenuation of RILF in vivo and in vitro by directly targeting PIWIL2 and activating purine metabolism.

Keywords: Radiation-induced lung fibrosis, Nrf2, PIWIL2, purine metabolism

Introduction

Radiotherapy is considered to be an effective way to treat thoracic cancers, such as lung cancer and breast cancer [1]. Radiation-induced lung fibrosis (RILF), the main complication of radiotherapy among thoracic cancer patients, not only limits the efficacy of radiotherapy but also seriously affects patients' quality of life [2]. Until now, little has been known about the exact molecular mechanism of the initiation and perpetuation of RILF. The lack of understanding about the pathogenesis of RILF hinders the development of effective therapeutic strategies for this kind of disease [3].

Recent studies showed that the NF-E2 related factor 2 (Nrf2) had a protective effect on radiation-induced lung injury [4]. Silencing of Nrf2 reduced the life span of mice after thoracic irradiation [5]. It was reported that overexpression of Nrf2 mitigated radiation-induced acute lung injury and inflammation [6-8]. In addition, the therapeutic effect of some drugs on RILF was mainly achieved by activating Nrf2 [9-11]. These findings confirm the value of Nrf2 in controlling RILF and are worthy of further study.

PIWI protein contains conserved PAZ and PIWI domains and has been suggested as a participant in stem cell self-renewal, spermatogenesis, RNA interference, and translation regulation in the process of evolution [12, 13]. In humans, four members of the PIWI subfamily have been identified: PIWIL1 (HIWI), PIWIL2 (HLI), PIWIL3 and PIWIL4 (HIWI2). As a member of the PIWI family, PIWIL2 is usually expressed in the testes but can be upregulated in somatic cells during DNA damage to promote repair by remodeling chromatin [14]. In cancer cells, the overexpression of PIWIL2 is related to the activation of signal transducer and activator of transcription 3 (STAT3)/Bcl-xL pathway [15]. Recent research has also shown that mouse

embryonic fibroblasts transfected with the PIWIL2 gene can produce cancer stem cell-like cell lines in vitro [16]. Elucidating the role of PIWIL2 in these studies will provide an opportunity to evaluate the potential function of PIWIL2 in RILF.

In the current study, we used wild-type and Nrf2 knockout ($Nrf2^{-/-}$) mice to study the suppression effect of Nrf2 on RILF. ChIP-seq assay and metabolomics analysis were performed to analyze the mechanism of action of Nrf2 in the attenuation of RILF. Our results suggest that Nrf2 protects against RILF by activating PIWIL2-induced purine metabolic reprogramming in lung tissue. These findings reveal the molecular mechanism of Nrf2-mediated RILF and provide evidence for reprogramming of purine metabolism in the repair of RILF.

Materials and methods

Cell culture and maintenance

The WI-38 cell line was purchased from the American Type Culture Collection (Manassas, VA, USA). The THP-1 cell line was purchased from ScienCell (Carlsbad, CA, USA). For cell maintenance, WI-38 cells were grown in MEM medium (Gibco, CA, USA) supplemented with 10% FBS and 1% penicillin/streptomycin. THP-1 cells were cultured in RPMI-1640 medium supplemented with 10% fetal bovine serum. The cells were incubated in a humidified atmosphere with 5% CO_2 at 37°C.

Lentivirus transfection

For knockdown of Nrf2 and PIWIL2, lentiviral shRNA vectors targeting human NFE2L2 and PIWIL2 genes, respectively, were purchased from HanBio (Shanghai, China). The sequence targeting NFE2L2 or PIWIL2 was synthesized and cloned into a lentiviral expression vector HBLV-GFP-PURO, which was named HBLV-h-NFE2L2 shRNA-GFP-PURO or HBLV-h-PIWIL2 shRNA-GFP-PURO. For overexpression of PIWIL2, a lentiviral expression vector named HBLV-h-PIWIL2-GFP-PURO was designed and synthesized by HanBio (Shanghai, China). The HBLV-GFP-PURO NC was used as a negative control. WI-38 and THP-1 cells were transfected with these indicated lentiviral expression vectors according to the manufacturer's instructions. Stable clonal cell lines were selected with 2.0 μg/μl puromycin. The efficiency of lentiviral transfection was evaluated by quantitative RT-PCR (qRT-PCR) and western blotting.

Irradiation

Cultured cells were irradiated with X-rays. The irradiation experiments were performed at room temperature with a single dose of 6 Gy. The dose rate applied in the experiments was 300 MU/min. X-rays were produced by a linear accelerator (Varian, CA, USA) of General Hospital of Ningxia Medical University.

qRT-PCR

RNA extraction and reverse transcription were carried out using TRIzol Reagent (Invitrogen) and Prime Script TM RT Master Mix (Perfect Real Time) kit (Takara, Japan) according to the manufacturers' protocols. qRT-PCR was performed in 20 μl reactions, including 2.0 μl of template cDNA, 6.4 μl of H_2O, 10 μl of 2× SYBR® Premix Ex Taq II (Tli RNaseH Plus), and 0.8 μl of forward and reverse primers (10 μM). The conditions for the qRT-PCR were as follows: 30 seconds at 95°C for one cycle, 40 cycles of 5 seconds at 95°C, and 30 seconds at 60°C, and melting curve analysis at 95°C for 5 seconds and 60°C for 1 minute. β-actin was used as an internal control to calculate the relative expression levels of indicated genes using the $2^{-\Delta\Delta Ct}$ method. The primers are listed in Table S1.

Western blotting

The cellular lysates were obtained using the radioimmunoprecipitation assay (RIPA) buffer according to the manual. The protein concentration was measured before the western blotting using the bicinchoninic acid (BCA) method. Subsequently, equal amounts of the protein samples were separated by SDS-PAGE and transferred onto polyvinylidene fluoride (PVDF) membranes. The membranes were then blocked with 5% nonfat milk followed by incubation with the primary antibodies. After the incubation, membranes were then processed with secondary antibody (horseradish peroxidase-conjugated goat anti-mouse or rabbit IgG, ZSGB-bio, China) after washing using PBS-tween buffer. Last, the protein was visualized by chemiluminescence (ECL) detection systems. GAPDH was selected as the internal control.

Enzyme-linked immunosorbent assay (ELISA)

TGF-β1 protein levels were measured in cell culture supernatant by a commercial TGF-β1 ELISA kit (Boster, Wuhan, China) following the manufacturer's instructions. The absorbance of samples was detected at 450 nm using a microplate reader (Bio-Tek, Vermont, USA). The obtained values were normalized to the corresponding cell culture supernatant of the control group during analysis.

Immunofluorescence

Immunofluorescence staining was carried out according to the manufacturer's instructions (FITC immunofluorescence detection kit, Sangon Biotech, China). Briefly, the cells were fixed with 4% paraformaldehyde for 20 minutes. After blocking with 5% normal donkey serum for 1 hour, the cells were then incubated overnight with anti-fibronectin (FN), anti-α-smooth muscle actin (α-SMA), and anti-collagen I antibody at 4°C. Then, cells were washed with phosphate-buffered saline (PBS) three times and incubated at room temperature for 2 hours with secondary FITC-conjugated anti-rabbit antibody. The fluorescence signal was detected by a Leica TCS SP2 confocal laser scanning microscope.

Animal model and study design

To establish the RILF model, on day 0, with the help of a holder, the right chest of mice was irradiated with linear accelerator (6 MV X-ray, 400 MU/min dose rate) with a single dose of 22.5 Gy. The mice in the control group were managed with the same method but were not irradiated. Eight-week-old female wild-type C57BL/6 mice and Nrf2 gene knockout ($Nrf2^{-/-}$) mice were purchased from the Model Animal Research Center of Nanjing University (Nanjing, China). In the phenotype experiment, 18 wild-type C57BL/6 mice of similar age and weight were randomly divided into 3 groups (each group had 6 mice): the control group, irradiation group, and CDDO-Me combined irradiation group. Six $Nrf2^{-/-}$ mice were taken as the fourth group and only received irradiation. The mice in the treatment group were administered with 600 ng CDDO-Me dissolved in 20 μl of saline every other day from the day -1 (days -1, 1, 3, 5, 7, and 9). The mice in the control group only received the same amount of normal saline. The mice were euthanized 12 weeks after irradiation, and the lung tissues of mice in each group were collected for the subsequent histology analysis. In the mechanism experiment, 24 wild-type C57BL/6 mice were randomly divided into 4 groups (each group had 6 mice): the control group, irradiation group, CDDO-Me combined irradiation group, and a group irradiated along with CDDO-Me and mycophenolate mofetil (MMF) (inosine-50-monophosphate dehydrogenase, IMPDH, inhibitor). The usage of CDDO-Me was the same as that in the phenotype experiments. The dose of MMF was 60 mg/kg. CDDO-Me was given by gavage administration every other day from day -1, a total of 6 times. MMF was given by gavage administration every two days from day 0, a total of 3 times. All animal experiments were conducted in accordance with the guiding principles provided by the Animal Ethics Committee of Ningxia Medical University (2014-0304).

Histopathological analysis

Lung tissues of mice were dehydrated with increasing concentrations of ethanol and embedded in paraffin, which was cut into 4-μm-thick slices, as described previously [17]. To evaluate the presence of fibrosis, lung tissue sections were stained with hematoxylin-eosin and Masson's trichrome staining. The Szapiel score, an index of histopathological changes, was used to evaluate and score the severity and extent of pulmonary fibrosis [18]. The content of collagen fibers in the lung tissue of the RILF model was detected by Masson's trichromatic staining. The Ashcroft score was used to characterize and score pulmonary fibrosis, which was stained by Masson's trichrome [19]. All the analyses were carried out by a skilled pathologist. The mean Szapiel and Ashcroft scores of each group of mice were determined, respectively.

Immunohistochemistry (IHC)

Paraffin-embedded lung tissue sections that were 4 μm thick were stained by IHC. The slices were incubated with 3% H_2O_2 to block the endogenous peroxidase following deparaffinization. After antigen retrieval and blocking, the slices were incubated with anti-FN, anti-α-SMA, and anti-collagen I polyclonal antibody at 4°C. The second antibody labeled by horseradish peroxidase was incubated at 37°C for 30

minutes, and the immunohistochemical reaction was observed according to the manufacturer's instructions with 3, 3'-diaminobenzidine (DAB) as a chromogenic agent. Subsequently, the slices were counterstained with hematoxylin-eosin and imaged with a light microscope (Olympus, Tokyo, Japan). IHC staining was evaluated by ImageJ software according to the AOD value.

Chromatin immunoprecipitation and sequencing (ChIP-Seq) analysis

ChIP-Seq analysis was performed as previously described with minor modifications [20]. Briefly, cells were harvested after the treatment with 50 nM CDDO-Me and chemically crosslinked using a final concentration of 1% formaldehyde for 15 minutes. Subsequently, cells were pelleted and lysed, and subsequently sonicated with a Diagenode Bioruptor on ice to generate 250-1,000 bp DNA fragments. Crosslinked protein/DNA was immunoprecipitated by Nrf2 antibody using preblocked magnetic beads. ChIP-seq libraries were prepared from two biological replicates by Illumina according to manufacturer's instructions. The completed libraries were quantified by Agilent 2100 Bioanalyzer. DNA libraries from input samples served as controls. The libraries were then sequenced on the Illumina HiSeq 4000 following the TruSeq Rapid SBS Kit protocol. Sequence reads were aligned to the human genome (HG19) using BOWTIE software (V2.1.0). The mapped reads were used for peak detection by MACS V1.4.2 (Model-based Analysis of ChIP-Seq) software. Significant ChIP-enriched regions (peaks) were identified by comparison of IP vs. input, using a *P* value threshold of 10^{-5}.

Metabolomics analysis

The metabolite extraction protocol was developed as previously described with minor modifications [21]. Briefly, cells were harvested and then dissolved in methanol/acetonitrile (1:1 v/v). After vortex and sonication, the samples were centrifuged at 20,000×g at 4°C for 10 minutes, and the obtained supernatant was injected into the UPLC/Q-TOF MS system for metabolite analysis. The compounds were separated by UHPLC using Agilent 1290 Infinity LC. UHPLC was performed with the following parameters: Mobile phase A: water with 25 mM ammonium acetate and 25 mM ammonium hydroxide; Mobile phase B: 100% acetonitrile. Gradient: initial 95% B at 0-1 minute; 95% to 65% B at 1-14 minutes; 65% to 40% B at 14-16 minutes; 40% B at 16-18 minutes; 40% to 95% B at 18-18.1 minutes; and 95% B at 18.1-23 minutes. Mass spectrometry was performed on the triple TOF™ 5600 equipped with ESI source, and mass range was set at m/z 600-1000. The following parameters were used for analysis: GS1: 60; GS2: 60; CUR: 30; and ISVF: 5500. Preprocessed data were exported to SIMCA-P 11.0 (Umetrics, Umea, Sweden) and used to establish multivariate statistical models by principal component analysis (PCA) and partial-least squares discriminant analysis (PLS-DA).

Statistical analysis

In the present study, the results are presented as the mean ± standard error. Data were analyzed using Student's t test. One-way analysis of variance (ANOVA) was used to determine the differences among multiple groups. Values were considered significantly different when P was less than 0.05. Statistical analyses were carried out using SPSS 18.0 Software Package (SPSS Inc., Chicago, USA) and GraphPad Prism 6.0 software (GraphPad Software, Inc., La Jolla, USA).

Results

The inhibitory effect of Nrf2 on RILF

Previously, we have reported that the activation of Nrf2, which was induced by CDDO-Me, alleviates RILF [17]. Based on this knowledge, this study established RILF models in vitro and in vivo to further explore the inhibitory effect of Nrf2 on RILF and its molecular mechanism. To investigate the biological function of Nrf2 in RILF protection, we first used shRNA to knock down Nrf2 in both WI-38 and THP-1 cells. Western blotting and qRT-PCR results showed that the levels of Nrf2 protein and mRNA in Nrf2-KD WI-38 (**Figure 1A**, **1B**) and THP-1 (**Figure 1C**, **1D**) cells were significantly lower than those in wild-type cells. TGF-β1 is a key factor in the development of lung fibrosis following irradiation [22]. Therefore, we then compared the expression level of TGF-β1 in different groups of WI-38 and THP-1 cells. We found that activation of Nrf2 inhibited the radiation-induced TGF-β1 level in the supernatant of both WI-38 and THP-1 cells. However, the radiation-

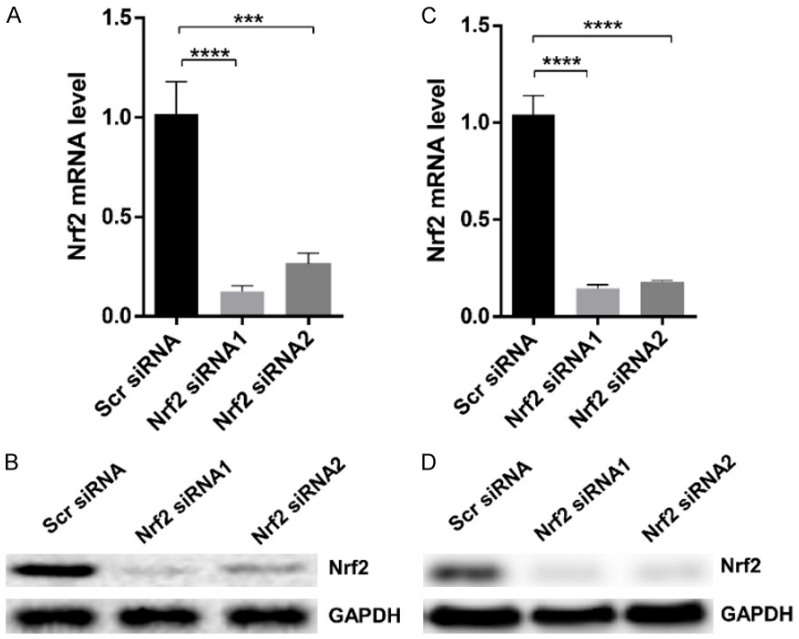

Figure 1. Nrf2 knockdown (Nrf2-KD) was confirmed at mRNA and protein levels by qRT-PCR and western blotting in WI-38 (A, B) and THP-1 (C, D) cells. ***P < 0.001 and ****P < 0.0001 by one-way analysis of variance followed by Tukey's post hoc test.

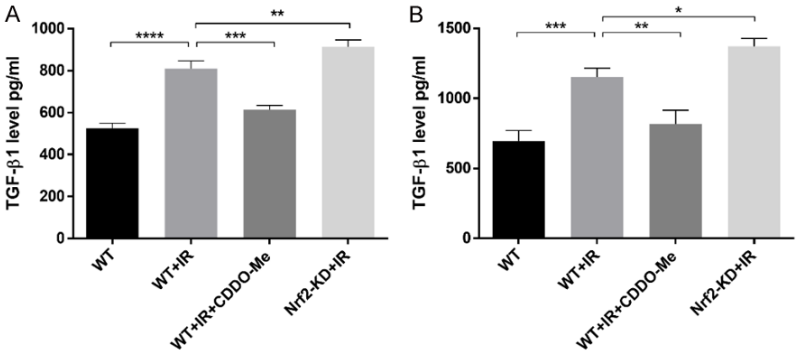

Figure 2. Effects of different levels of Nrf2 on the production of transforming growth factor-β1 (TGF-β1) in WI-38 (A) and THP-1 (B) cells after irradiation. The wild-type (WT) cells were irradiated (IR) (6 Gy) in the presence or absence of 50 nM CDDO-Me. The irradiated Nrf2-KD cells were exposed to the same dose of X-ray as WT cells. The expression levels of TGF-β1 in the culture supernatant of WI-38 (A) and THP-1 (B) cells were detected by enzyme-linked immunosorbent assay (ELISA). *P < 0.05, **P < 0.01, ***P < 0.001, and ****P < 0.0001 by one-way analysis of variance followed by Tukey's post hoc test.

induced TGF-β1 level of Nrf2-KD WI-38 (**Figure 2A**) and THP-1 (**Figure 2B**) cells was significantly higher than that of wild-type cells. To further confirm the important role of Nrf2 in RILF, we quantitatively studied the expression levels of FN, α-SMA, and collagen I in different groups of WI-38 and THP-1 cells using immunofluorescence staining method. Irradiation significantly elevated the expression level of FN, α-SMA, and collagen I. After CDDO-Me treatment, the levels of FN, α-SMA and collagen I were decreased. Conversely, inhibition of Nrf2 increased the expression of these three profibrotic factors in irradiated-WI-38 (**Figure 3**) and THP-1 cells (**Figure 4**).

To evaluate the inhibitory efficacy of Nrf2 on RILF in vivo, lung tissue samples of RILF mice were collected and stained with hematoxylin-eosin and Masson's trichrome. Irradiation caused extensive subpleural collagen accumulation in the lung tissues of wild-type and Nrf2$^{-/-}$ mice. The above pathological changes in Nrf2$^{-/-}$ mice were more serious than those in the wild-type group. However, these fibrotic effects can be limited by activation of Nrf2 via CDDO-Me. The representative images are shown in **Figure 5**. The Szapiel scores of hematoxylin-eosin staining and the Ashcroft scores of Masson's trichrome staining also supported that activation of Nrf2 inhibited the deposition of collagen in lung tissues of RILF mice (**Figure 5**). In addition, the protein levels of FN, α-SMA and collagen I in lung tissues, which were detected by IHC, also confirmed that the loss of Nrf2 aggravated RILF, while the activation of Nrf2 had a protective effect on RILF (**Figure 6**). Collectively, these data indicate that Nrf2 plays an important role in the pathogenesis of RILF. Upregulation of Nrf2 eliminates RILF in vitro and in vivo.

Nrf2 exerts a protective role against RILF by activating PIWIL2

To explore the molecular mechanism of Nrf2 in controlling RILF, the target genes of Nrf2 were identified by ChIP-seq. Compared with the neg-

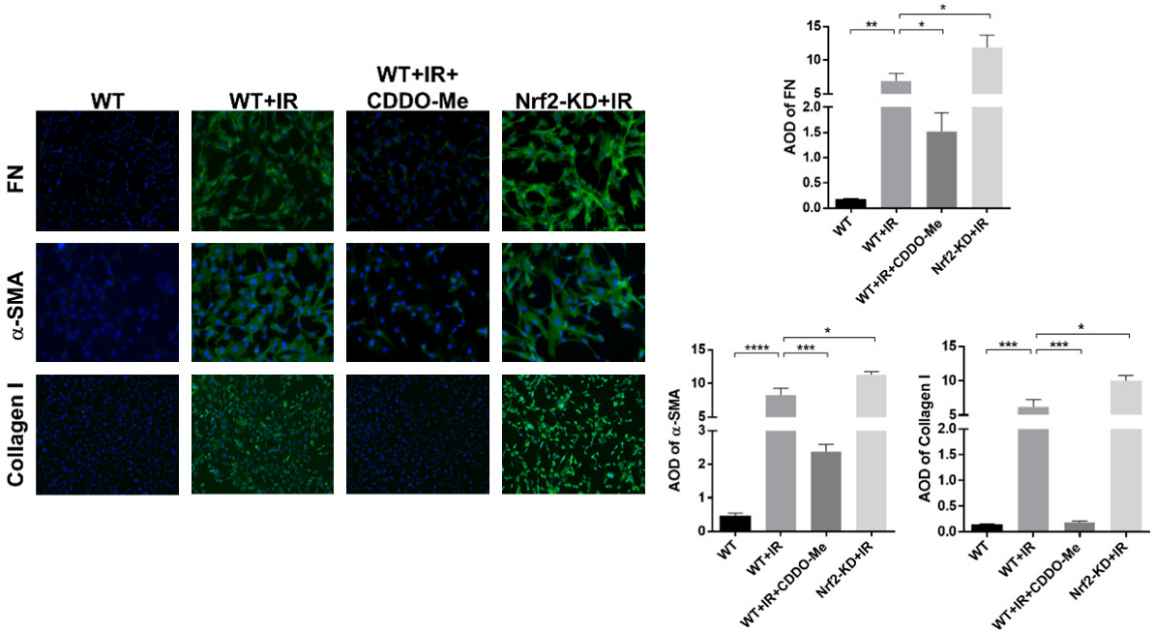

Figure 3. Effects of different levels of Nrf2 on the expression of profibrotic genes in irradiated WI-38 cells. The wild-type (WT) WI-38 cells were irradiated (IR) (6 Gy) in the presence or absence of 50 nM CDDO-Me. The irradiated Nrf2-KD WI-38 cells were exposed to the same dose of X-ray as WT cells. The expression levels of fibronectin (FN), α-smooth muscle actin (α-SMA) and collagen I were detected by immunofluorescence staining. *P < 0.05, **P < 0.01, ***P < 0.001, and ****P < 0.0001 by one-way analysis of variance followed by Tukey's post hoc test.

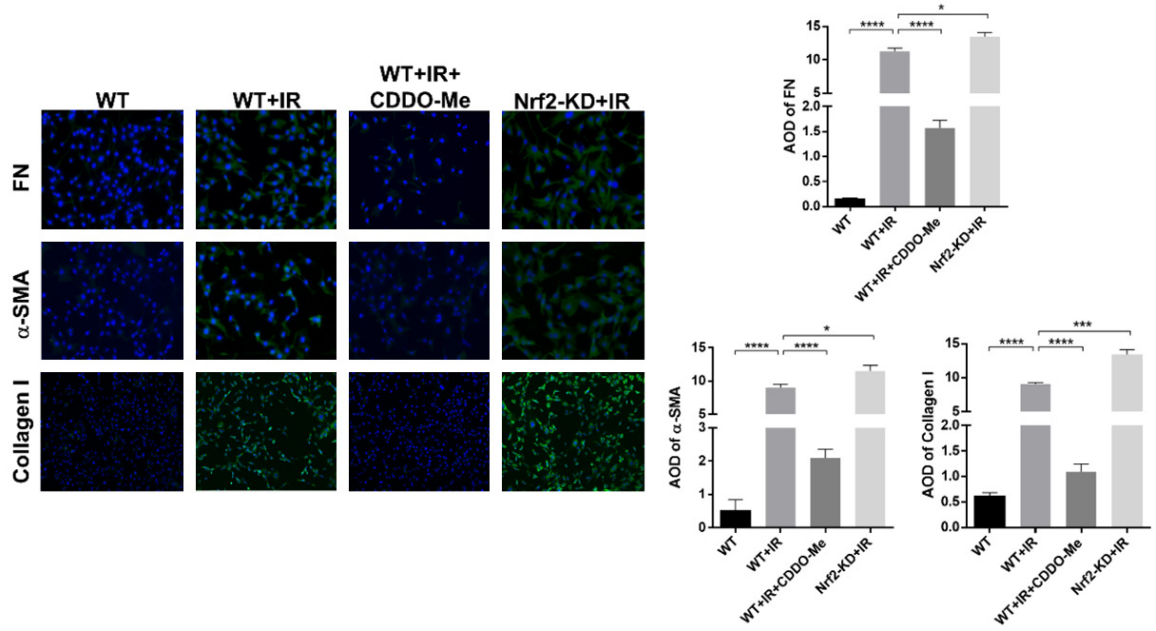

Figure 4. Effects of different levels of Nrf2 on the expression of profibrotic genes in irradiated THP-1 cells. The wild-type (WT) THP-1 cells were irradiated (IR) (6 Gy) in the presence or absence of 50 nM CDDO-Me. The irradiated Nrf2-KD THP-1 cells were exposed to the same dose of X-ray as WT cells. The expression levels of fibronectin (FN), α-smooth muscle actin (α-SMA) and collagen I were detected by immunofluorescence staining. *P < 0.05, **P < 0.01, ***P < 0.001, and ****P < 0.0001 by one-way analysis of variance followed by Tukey's post hoc test.

ative control, 1180 genomic regions (peaks) were significantly enriched ($P < 10^{-5}$). **Figure 7A** shows the peak distribution around transcription start sites (TSS) (±5 kb to TSS). The peaks

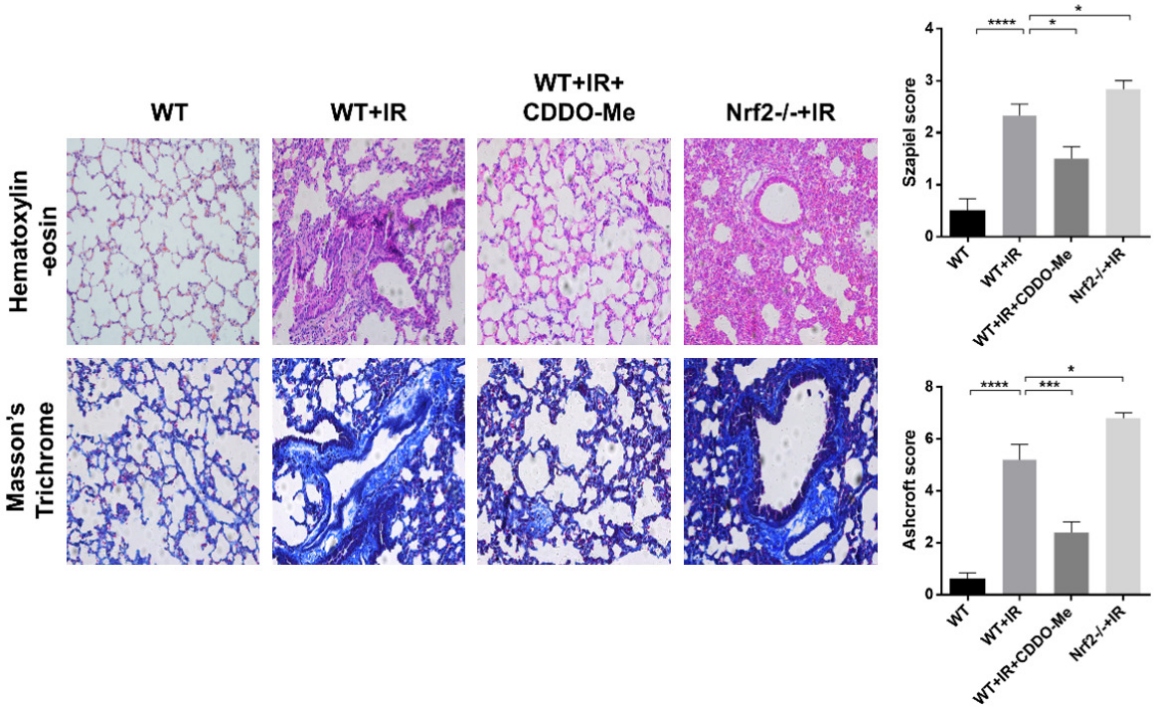

Figure 5. Effects of different levels of Nrf2 on the pathological changes associated with radiation-induced lung fibrosis (RILF). Female wild-type (WT) C57BL/6 mice received 22.5 Gy thoracic irradiation (IR) and were treated with CDDO-Me or vehicle. Female Nrf2 knockout ($Nrf2^{-/-}$) mice also received 22.5 Gy thoracic IR. Hematoxylin-eosin staining and Masson's trichrome staining were performed in the lungs of mice in the WT group, WT+IR group, WT+IR+CDDO-Me group and $Nrf2^{-/-}$+IR group. Histopathological sections were evaluated by a semiquantitative scoring method. The Szapiel score and Ashcroft score are shown as the mean ± standard error of 6 mice in each group.*P < 0.05, ***P < 0.001, and ****P < 0.0001 by one-way analysis of variance followed by Tukey's post hoc test.

in the range from -2 kb to +2 kb around the corresponding gene TSS were annotated using the UCSC RefSeq database. A total of 56 genes were annotated as target genes of Nrf2 ($P < 10^{-5}$). The genes with higher fold enrichment value, including POLN, PIWIL2, CDHR3, GSTA4, CYSLTR2, LILRB1, SNX16, COL6A1 and USP17, were selected as candidate genes and further validated in the qRT-PCR assay. The fold enrichment value of these nine genes is shown in **Figure 7B**. The qPCR assay results showed that Nrf2 could drive the transcriptional activity of PIWIL2, CDHR3, GSTA4, CYSLTR2, SNX16, COL6A1 and USP17 (**Figure 7C**). Among the top three changed genes, which had been verified in the qRT-PCR assay, only PIWIL2 had a potential role in the inhibition of RILF [23]. Therefore, we chose PIWIL2 as the target gene of Nrf2 for the subsequent analysis.

Next, PIWIL2 worked as the target gene of Nrf2 and was verified in vivo. The expression of Nrf2 and PIWIL2 in the lung tissue of wild-type and $Nrf2^{-/-}$ mice was analyzed by the IHC method (**Figure 8**). The results showed that activation of Nrf2 elevated the level of PIWIL2 in the lung tissue of wild-type mice. A significant decrease in PIWIL2 was detected in the lung tissues of $Nrf2^{-/-}$ mice.

Last, we assessed the role of PIWIL2 in Nrf2-mediated RILF reduction. We used lentivirus expression vector and lentivirus shRNA vector to overexpress and downregulate the expression of PIWIL2 in WI-38 cells. These results had been confirmed in both western blotting and qRT-PCR experiments (**Figure 9A**, **9B**). After that, we evaluated the impact of PIWIL2 on radiation-induced TGF-β1 expression levels. As shown in **Figure 9C**, activation of Nrf2 inhibited the production of TGF-β1 in WI-38 cells triggered by irradiation. However, shRNA-mediated PIWIL2 knockdown reversed the protective effect of Nrf2. Interestingly, similar to Nrf2, overexpression of PIWIL2 also significantly inhibited the TGF-β1 level in WI-38 cells induced by irradiation (**Figure 9C**). In the evaluation of the pro-fibrotic factor expression levels using

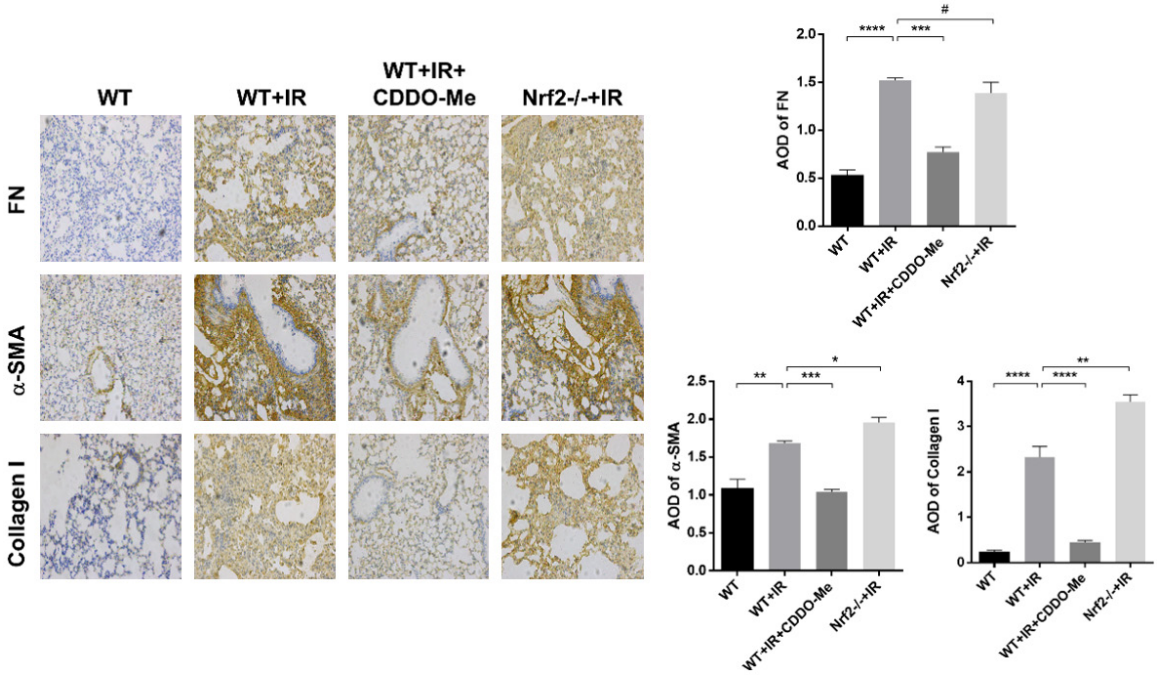

Figure 6. Effects of different levels of Nrf2 on the expression of profibrotic genes in irradiated mice. Female wild-type (WT) C57BL/6 mice received 22.5 Gy thoracic irradiation (IR) and were treated with CDDO-Me or vehicle. Female Nrf2 knockout ($Nrf2^{-/-}$) mice received 22.5 Gy thoracic IR. The expression levels of profibrotic factors, such as fibronectin (FN), α-smooth muscle actin (α-SMA), and collagen I, were detected by immunohistochemistry. # no significant difference, *P < 0.05, **P < 0.01, ***P < 0.001, and ****P < 0.0001 by one-way analysis of variance followed by Tukey's post hoc test.

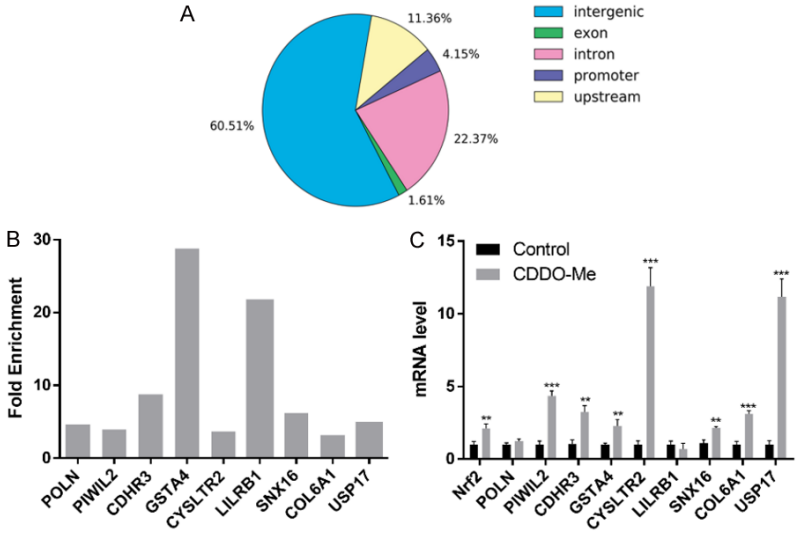

Figure 7. The target genes of Nrf2 were analyzed by ChIP-seq and verified by qRT-PCR. The distribution of the peaks annotated in the ChIP-seq assay over important genomic features (A). The fold enrichment value of the candidate genes screened from ChIP-seq assay (B). The qRT-PCR method was used to analyze the mRNA expression level of these candidate genes in WI-38 cells before and after 50 nM CDDO-Me treatment (C). **P < 0.01 and ***P < 0.001 by one-way analysis of Student's t-test.

immunofluorescence staining, the results showed that CDDO-Me downregulated the level of FN, α-SMA and collagen I in WI-38 cells following irradiation. When PIWIL2 was knocked down in WI-38 cells, the anti-fibrotic effect of Nrf2 could be significantly reversed. In addition, the expression levels of these pro-fibrotic factors could also be suppressed by the activation of PIWIL2 (**Figure 10**). These data suggest that Nrf2 plays a protective role in RILF by targeting PIWIL2.

PIWIL2 triggers the reprogramming of purine metabolism in WI-38 cells

Considering the pivotal role of the altered metabolic

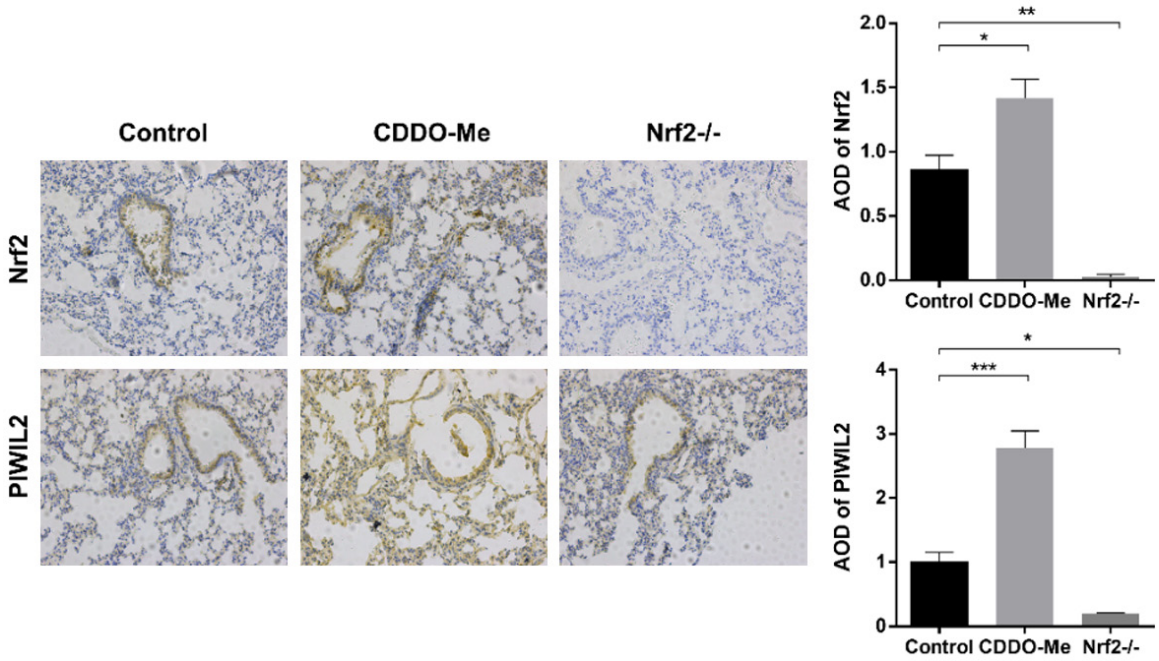

Figure 8. PIWIL2 as the target gene of Nrf2 has been verified in vivo. Female wild-type (WT) C57BL/6 mice were exposed to six doses of CDDO-Me (600 ng) or vehicle. Female Nrf2 knockout ($Nrf2^{-/-}$) mice were also used in this experiment. The expression level of Nrf2 and PIWIL2 was detected by immunohistochemistry. *P < 0.05, **P < 0.01, and ***P < 0.001 by one-way analysis of variance followed by Tukey's post hoc test.

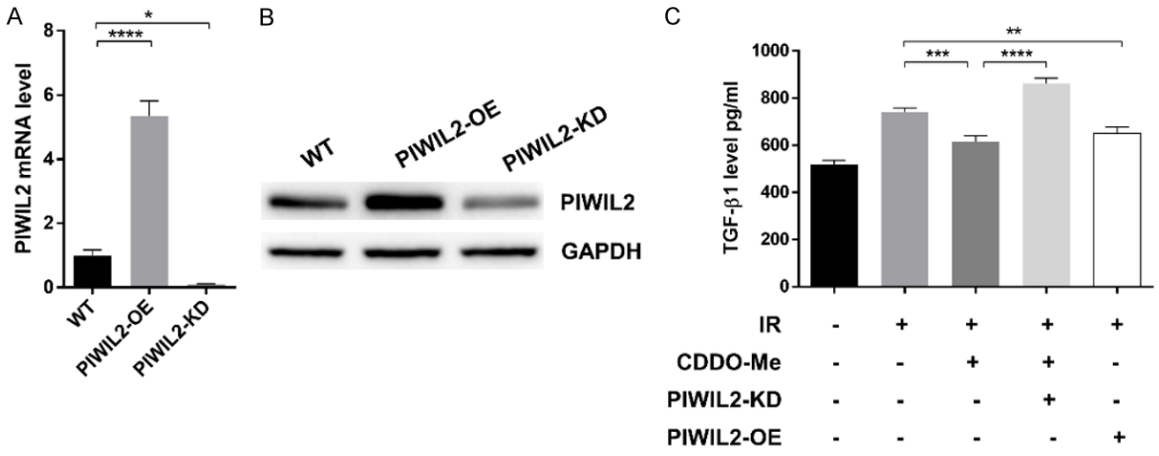

Figure 9. The role of different PIWIL2 expression levels on the production of transforming growth factor-β1 (TGF-β1) in WI-38 cells after irradiation. PIWIL2 overexpression (PIWIL2-OE) and knockdown (PIWIL2-KD) were confirmed at the mRNA (A) and protein (B) levels by qRT-PCR and western blotting in WI-38 cells. The wild-type (WT) WI-38 cells were irradiated (IR) (6 Gy) in the presence or absence of 50 nM CDDO-Me. The PIWIL2-KD WI-38 cells were treated with 50 nM CDDO-Me following 6 Gy of IR. PIWIL2-OE WI-38 cells were only irradiated by 6 Gy X-rays. The expression levels of transforming growth factor-β1 (TGF-β1) in the culture supernatant were detected by enzyme-linked immunosorbent assay (ELISA) (C). *P < 0.05, **P < 0.01, ***P < 0.001, and ****P < 0.0001 by one-way analysis of variance followed by Tukey's post hoc test.

activities in the pathogenesis of RILF [24], we explored whether PIWIL2 exerted an antifibrotic role by reprogramming the metabolic pathways (**Figure 11**). To do so, we performed metabolomics analysis on wild-type and PIWIL2-OE WI-38 cells. Interestingly, PIWIL2 overexpression significantly increased intracellular ribose-5P, purine nucleotides, and their intermediates, such as inosine 5'-monophosphate (IMP), guanosine 5'-monophosphate (GMP), guanosine,

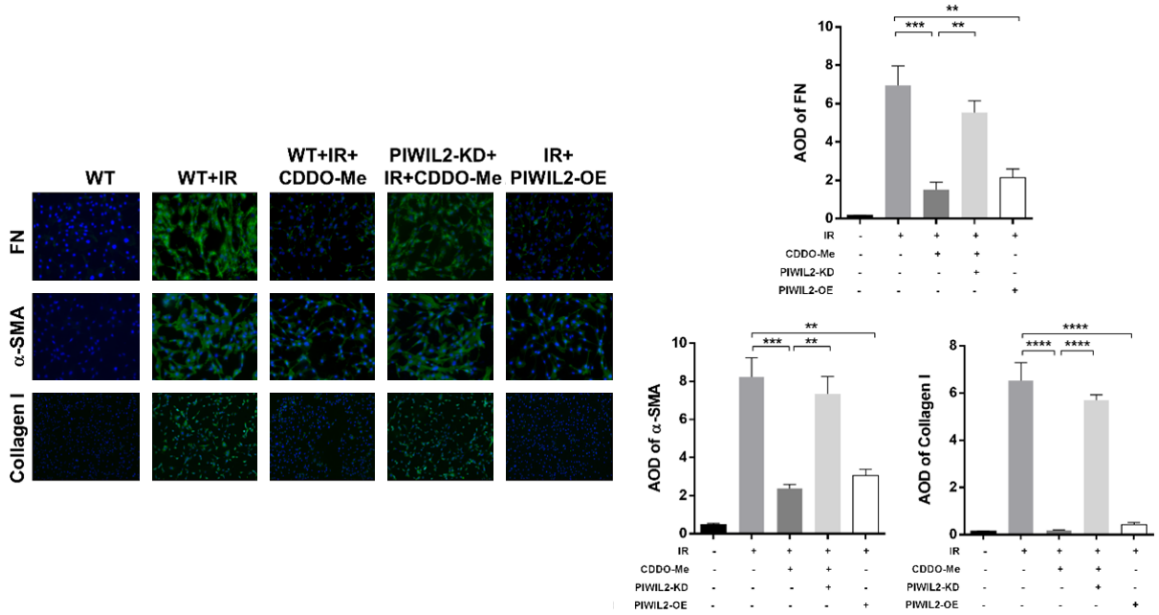

Figure 10. Effects of different levels of PIWIL2 on the expression of pro-fibrotic genes in irradiated WI-38 cells. The wild-type (WT) WI-38 cells were irradiated (IR) (6 Gy) in the presence or absence of 50 nM CDDO-Me. The PIWIL2 knockdown (PIWIL2-KD) WI-38 cells were treated with 50 nM CDDO-Me following 6 Gy of IR. PIWIL2-overexpressing (PIWIL2-OE) WI-38 cells were irradiated by 6 Gy X-rays only. The expression levels of fibronectin (FN), α-smooth muscle actin (α-SMA) and collagen I were detected by immunofluorescence staining. **P < 0.01, ***P < 0.001, and ****P < 0.0001 by one-way analysis of variance followed by Tukey's post hoc test.

adenosine monophosphate (AMP), inosine, hypoxanthine, adenosine 5'-diphosphate (ADP), xanthine, adenosine, and adenosine 5'-triphosphate (ATP), suggesting that PIWIL2 overexpression might promote the de novo purine synthesis pathway (**Figure 12A**, **12B**). To further confirm this result, we used targeted metabolic assay to determine the relative levels of serine, nucleoside intermediate (AICAR) and nucleoside monophosphate (IMP and GMP) between wild-type and PIWIL2-OE WI-38 cells. The overexpression of PIWIL2 elevated the levels of AICAR, IMP and GMP, suggesting that the alleviation of RILF driven by PIWIL2 may require higher demand for purine biosynthesis (**Figure 12C**). Furthermore, we evaluated the mRNA level of the critical rate-limiting enzymes needed to encode in the purine biosynthesis pathway by qPCR. We found that the expression of IMPDH1 and IMPDH2 in PIWIL2-OE WI-38 cells was significantly higher than that in wild-type cells, while the expression of IMPDH2 in PIWIL2-KD WI-38 cells was significantly decreased (**Figure 13A**). Taken together, these data suggest that PIWIL2 triggers the reprogramming of purine metabolism in WI-38 cells.

The role of Nrf2/PIWIL2/purine metabolism axis in controlling RILF

To further confirm the role of the Nrf2/PIWIL2/purine metabolism axis in the inhibition of RILF, WI-38 cells were irradiated, managed with CDDO-Me, and transfected with lentivirus for PIWIL2 gene knockdown and overexpression, and MMF and ELISA were subsequently performed. As shown in **Figure 13B**, transfection of PIWIL2 shRNA dramatically inhibited the downregulation effect of CDDO-Me on the level of TGF-β1 in the supernatant of irradiated WI-38 cells. Upregulation of PIWIL2 alone also inhibited the elevation of TGF-β1 induced by irradiation. Furthermore, MMF could reverse the inhibitory effect of Nrf2 or PIWIL2 on radiation-induced TGF-β1. To further verify the role of purine metabolism in attenuating RILF, we combined using CDDO-Me and MMF in RILF mice. As expected, MMF significantly reversed the therapeutic effect of CDDO-Me in the lungs of C57BL/6 mice (**Figure 14**). In summary, these data suggest that the activation of the Nrf2/PIWIL2/purine metabolic axis has a therapeutic effect on RILF.

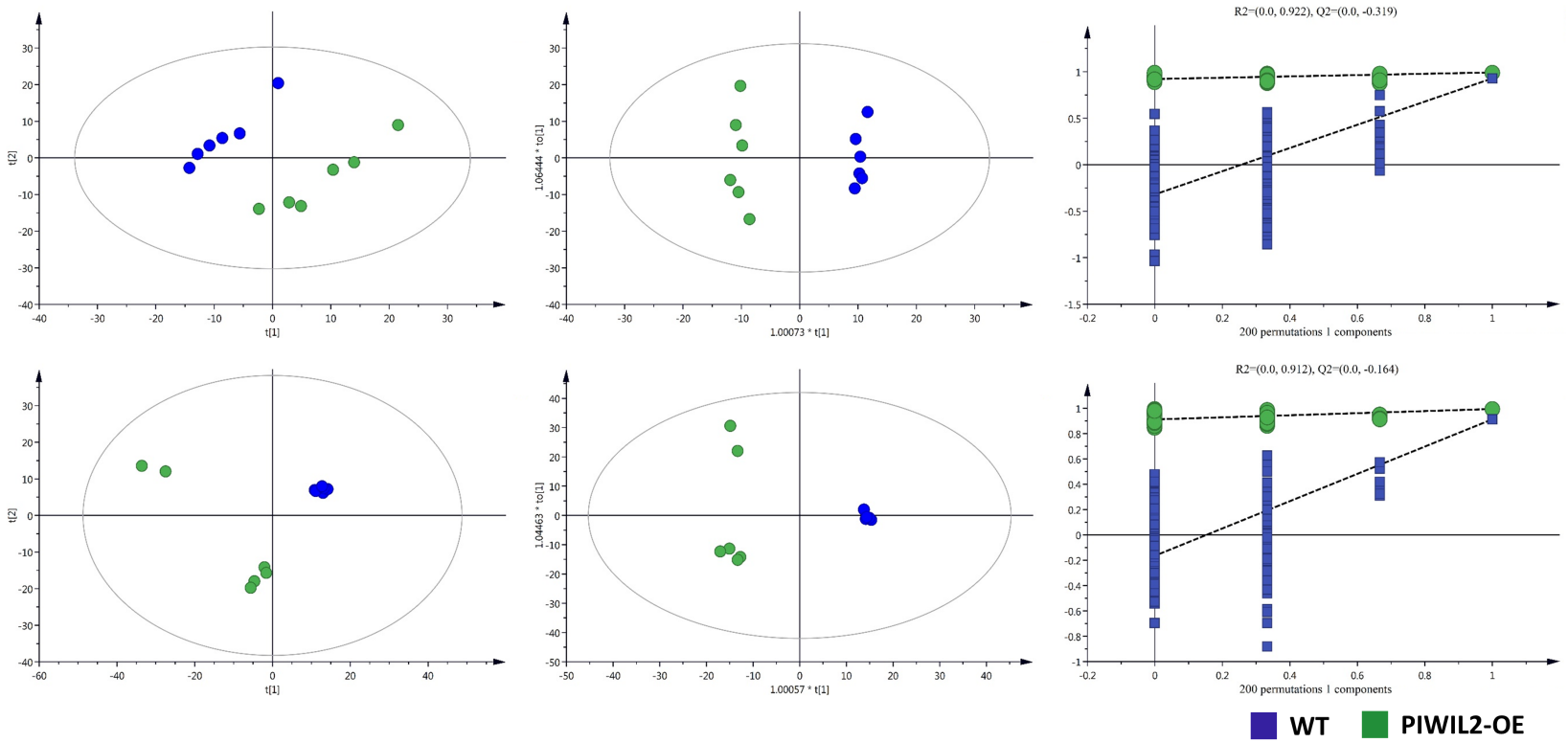

Figure 11. Metabolomics analysis of PIWIL2-overexpressing (PIWIL2-OE) WI-38 cells. The principal component analysis (PCA) score plots, orthotopic partial least-squares discriminant analysis (OPLS-DA) score plots, and permutation tests for the OPLS-DA score plots of positive (First line) and negative (Second line) model.

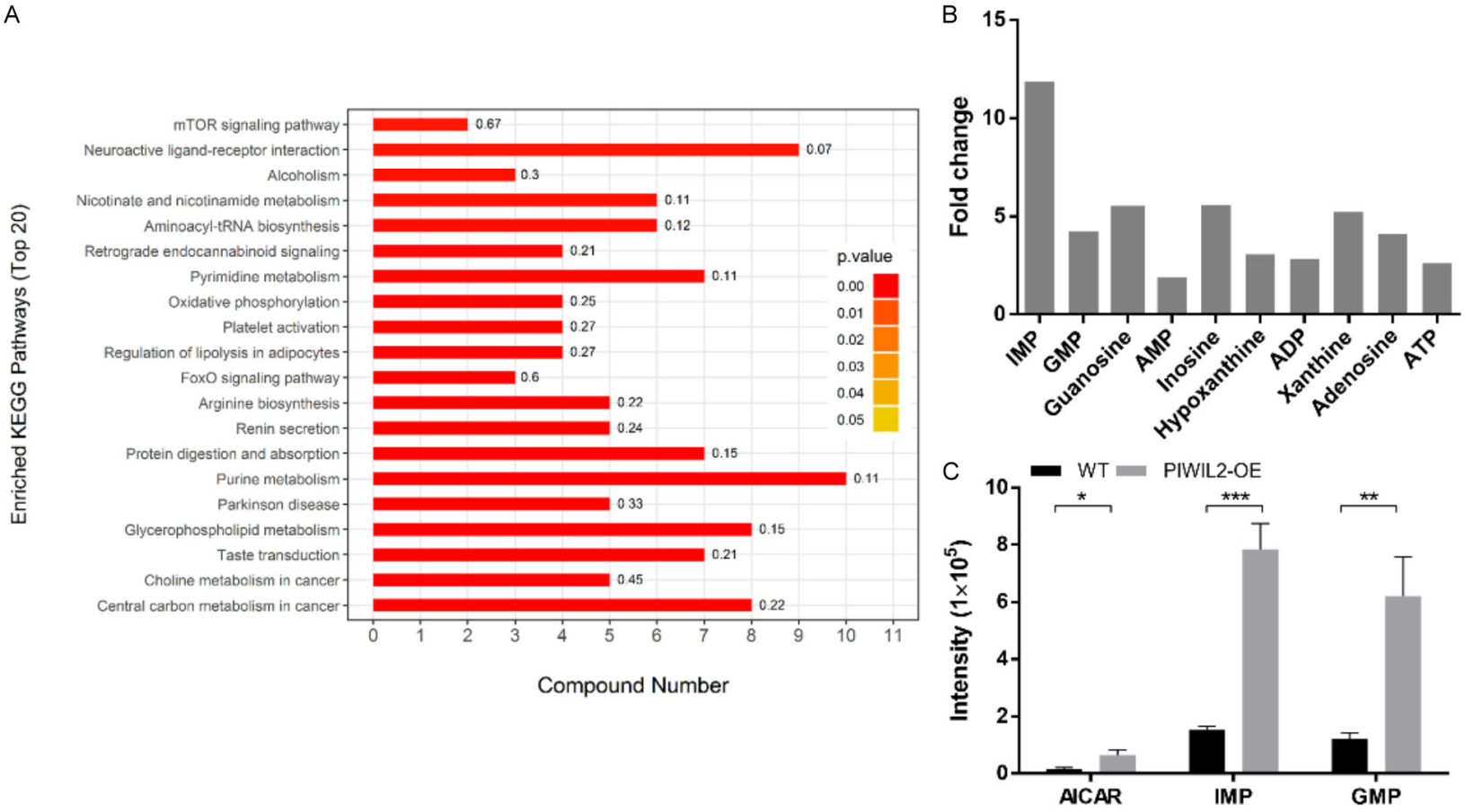

Figure 12. Effect of PIWIL2 overexpression on purine metabolism in WI-38 cells. KEGG pathways enriched in the metabolomic analysis of PIWIL2-OE WI-38 cells (A). Fold changes of metabolites related to purine metabolism in PIWIL2-OE WI-38 cells (B). Targeted metabolomics assay was performed to measure the relative levels of L-serine, nucleoside intermediate (AICAR), and nucleoside monophosphates (IMP and GMP) between PIWIL2-OE and WT WI-38 cells (C). *P < 0.05, **P < 0.01, and ***P < 0.001 by Student's t-test.

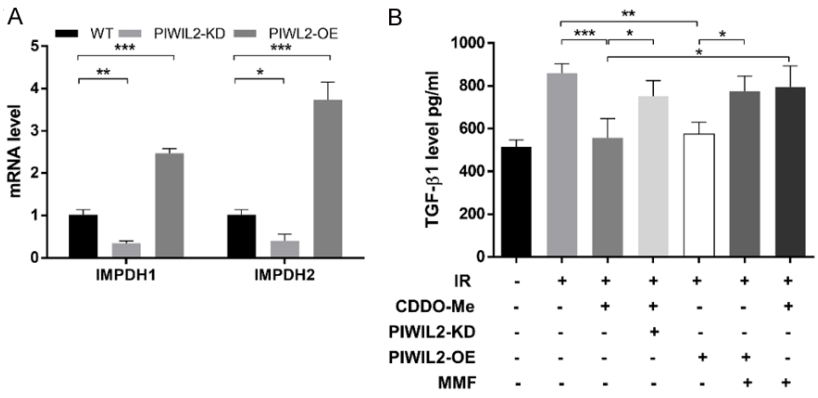

Figure 13. The effects of PIWIL2 overexpression (PIWIL2-OE) and knockout (PIWIL2-KD) on the expression of purine metabolism rate-limiting enzymes were analyzed by qRT-PCR (A). The wild-type (WT) WI-38 cells were irradiated (6 Gy) in the presence or absence of 50 nM CDDO-Me. The PIWIL2-KD WI-38 cells were treated with 50 nM CDDO-Me following 6 Gy of irradiation (IR). The PIWIL2-OE WI-38 cells were irradiated (6 Gy) in the presence or absence of 5 mM mycophenolate mofetil (MMF). The WT WI-38 cells treated with CDDO-Me and MMF following 6 Gy X-ray exposure. The expression levels of transforming growth factor-β1 (TGF-β1) in the culture supernatant were detected by enzyme-linked immunosorbent assay (ELISA) (B). *P < 0.05, **P < 0.01, and ***P < 0.001 by one-way analysis of variance followed by Tukey's post hoc test.

Discussion

Although RILF is the main complication of radiotherapy for thoracic cancer patients, there is a lack of effective treatment at present. An increasing number of studies have shown that Nrf2 plays a role in the initiation and development of RILF [5-9]. However, before using Nrf2 as a diagnostic or therapeutic target, it is particularly important to understand the regulatory mechanism of Nrf2 in RILF.

In this study, we first evaluated the effect of different levels of Nrf2 on the pathogenesis of RILF in vitro and in vivo. In in vitro studies, we found that Nrf2 deficiency aggravated RILF by upregulating TGF-β1 and profibrotic genes, including FN, α-SMA and collagen I. The overexpression of Nrf2 induced by CDDO-Me could reverse the above effects. In in vivo studies, the pathological changes in RILF in $Nrf2^{-/-}$ mice were much more severe than those in wild-type mice. However, the RILF in mice could be attenuated by Nrf2 overexpression. It is suggested that Nrf2 exerts the protective effect on RILF. In the subsequent study, we used ChIP-seq method to screen and to verify the downstream target genes of Nrf2. According to the results of ChIP-seq assay, the literature review, and the preliminary experiment, PIWIL2 was selected as the downstream molecule of Nrf2 for further study.

PIWIL2 is a cancer/testicular antigen protein involved in a variety of biological processes, including gametogenesis, stem cell self-renewal, RNA silencing and translation control [13]. Although there is no direct evidence, some studies have shown that PIWIL2 has potential value in the prevention and control of RILF. PIWIL2 triggers ubiquitin-controlled TGF-β receptor degradation by interacting with heat shock protein 90, thus downregulating TGF-β signal transduction [23]. PIWIL2 can also save cells from various stress damages and promote cell survival [25, 26]. In addition, it is reported that PIWIL2 facilitates the repair of DNA damage by mediating chromatin relaxation [14]. In the current study, we found that PIWIL2 was the downstream target of Nrf2 and suppressed RILF. PIWIL2 gene knockdown led to the reverse of the therapeutic effect of CDDO-Me on RILF. Like Nrf2, PIWIL2 overexpression also had a therapeutic effect on RILF. Accumulating evidence shows that cellular metabolism is involved in the development of RILF [24]. Therefore, we performed metabolomics analysis in the subsequent study to clarify the mechanisms of PIWIL2 against RILF. We found that PIWIL2 inhibited RILF by reprogramming purine metabolism.

Purines are not only the components of a biomolecule but also the cofactors that provide energy and drive the signal transduction of cellular processes [27]. Purine metabolism includes de novo purine biosynthesis pathway, purine rescue pathway and degradation and maintains the cell pools of adenylate and guanylate through the synthesis and degradation of purine nucleotides [28]. Therefore, purine metabolism is related to several biochemical processes, including the pathogenesis of lung injury. In the model of lung inflammation induced by lipopolysaccharide (LPS)-containing allergens, studies have confirmed that acetyl salicylic acid (ASA) plays a therapeutic role through adenosine [29]. Inosine is the key

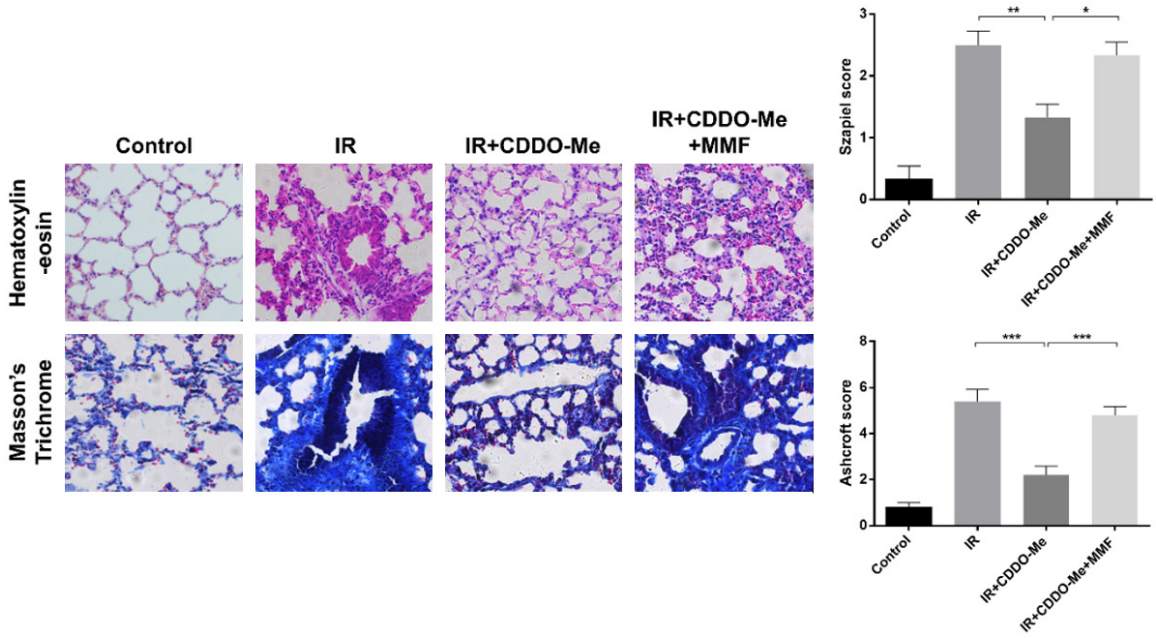

Figure 14. The lung tissues of mice in the control group, irradiation (IR) group, IR+CDDO-Me group and IR+CDDO-Me+ mycophenolate mofetil (MMF) group were stained with hematoxylin-eosin and Masson's trichrome staining. Histopathological sections were evaluated by a semiquantitative scoring method. The Szapiel score and Ashcroft score are shown as the mean ± standard error of 6 mice in each group. *P < 0.05, **P < 0.01, and ***P < 0.001 by one-way analysis of variance followed by Tukey's post hoc test.

metabolite of purine metabolism. Adenosine is converted to inosine under the action of purine catabolism enzyme adenosine deaminase (ADA). Inosine has been shown to be associated with inflammation in animal models of bronchial asthma [30]. In addition, mangiferin is an anti-inflammatory compound that reduces lung injury and protects organs in mice with sepsis by increasing the synthesis of inosine [31]. Furthermore, the vascular protective effects of adenosine, inosine and guanosine have been demonstrated in the rat model of hemolytic induced pulmonary hypertension [32]. In the current study, our metabolomics analysis showed that the levels of IMP and GMP in PIWIL2-OE WI-38 cells were significantly higher than those in wild-type cells, suggesting that the repair of RILF may require higher demand for purine biosynthesis. Additionally, we found that PIWIL2 increased the expression of IMPDH1 and IMPDH2, the rate-limiting enzymes of GMP synthesis in WI-38 cells. This study also confirmed that the inhibitory effect of MMF on IMPDH1 and IMPDH2 reversed the therapeutic effect of Nrf2 or PIWIL2 in vitro and in vivo. It is suggested that purine metabolism is involved in the alleviation of RILF and that the Nrf2/PIWIL2/purine metabolism axis contributes to the control of RILF.

Conclusion

We studied the role and underlying mechanism of Nrf2 in the alleviation of RILF. We demonstrated that Nrf2 significantly inhibited RILF by acting as a positive upstream regulator of PIWIL2. Moreover, the activation of PIWIL2 triggered the alteration of purine metabolism and initiated the repair of RILF. Artificial regulation of the Nrf2/PIWIL2/purine metabolic axis may be a new way to control RILF. This study expands our knowledge on the antifibrotic effect of Nrf2 and is the first study to evaluate the demand for purine synthesis in the process of RILF repair.

Acknowledgements

This work is supported by National Natural Science Foundation of China (81460477) and First Class Discipline (Clinical Medicine) Project of Ningxia (NXYLXK2017A05). Medical writing support was provided by editors from American Journal Experts Company.

Disclosure of conflict of interest

None.

Address correspondence to: Dr. Yan-Yang Wang, Department of Radiation Oncology, General Hospital of Ningxia Medical University, Yinchuan 750004, Ningxia, China; Cancer Institute, Ningxia Medical University, Yinchuan 750004, Ningxia, China. Tel: +86-951-6743-975; E-mail: fdwyy1981@hotmail.com

References

[1] Lee VH, Yang L, Jiang Y and Kong FS. Radiation therapy for thoracic malignancies. Hematol Oncol Clin North Am 2020; 34: 109-125.

[2] Hanania AN, Mainwaring W, Ghebre YT, Hanania NA and Ludwig M. Radiation-induced lung injury: assessment and management. Chest 2019; 156: 150-162.

[3] Giuranno L, Ient J, De Ruysscher D and Vooijs MA. Radiation-induced lung injury (RILI). Front Oncol 2019; 9: 877.

[4] Cameron BD, Sekhar KR, Ofori M and Freeman ML. The role of Nrf2 in the response to normal tissue radiation injury. Radiat Res 2018; 190: 99-106.

[5] Travis EL, Rachakonda G, Zhou X, Korhonen K, Sekhar KR, Biswas S and Freeman ML. NRF2 deficiency reduces life span of mice administered thoracic irradiation. Free Radic Biol Med 2011; 51: 1175-1183.

[6] Tian X, Wang F, Luo Y, Ma S, Zhang N, Sun Y, You C, Tang G, Li S, Gong Y and Xie C. Protective role of nuclear factor-erythroid 2-related factor 2 against radiation-induced lung injury and inflammation. Front Oncol 2018; 8: 542.

[7] Traver G, Mont S, Gius D, Lawson WE, Ding GX, Sekhar KR and Freeman ML. Loss of Nrf2 promotes alveolar type 2 cell loss in irradiated, fibrotic lung. Free Radic Biol Med 2017; 112: 578-586.

[8] Duru N, Gernapudi R, Zhang Y, Yao Y, Lo PK, Wolfson B and Zhou Q. NRF2/miR-140 signaling confers radioprotection to human lung fibroblasts. Cancer Lett 2015; 369: 184-191.

[9] Yu J, Zhu X, Qi X, Che J and Cao B. Paeoniflorin protects human EA.hy926 endothelial cells against gamma-radiation induced oxidative injury by activating the NF-E2-related factor 2/heme oxygenase-1 pathway. Toxicol Lett 2013; 218: 224-234.

[10] Mathew B, Jacobson JR, Siegler JH, Moitra J, Blasco M, Xie L, Unzueta C, Zhou T, Evenoski C, Al-Sakka M, Sharma R, Huey B, Bulent A, Smith B, Jayaraman S, Reddy NM, Reddy SP, Fingerle-Rowson G, Bucala R, Dudek SM, Natarajan V, Weichselbaum RR and Garcia JG. Role of migratory inhibition factor in age-related susceptibility to radiation lung injury via NF-E2-related factor-2 and antioxidant regulation. Am J Respir Cell Mol Biol 2013; 49: 269-278.

[11] Bian C, Qin WJ, Zhang CY, Zou GL, Zhu YZ, Chen J, Zhao R, Wang YY and Zhe H. Thalidomide (THD) alleviates radiation induced lung fibrosis (RILF) via down-regulation of TGF-beta/Smad3 signaling pathway in an Nrf2-dependent manner. Free Radic Biol Med 2018; 129: 446-453.

[12] Aravin AA, Hannon GJ and Brennecke J. The Piwi-piRNA pathway provides an adaptive defense in the transposon arms race. Science 2017; 318: 761-764.

[13] Ponnusamy M, Yan KW, Liu CY, Li PF and Wang K. PIWI family emerging as a decisive factor of cell fate: an overview. Eur J Cell Biol 2017; 96: 746-757.

[14] Yin DT, Wang Q, Chen L, Liu MY, Han C, Yan Q, Shen R, He G, Duan W, Li JJ, Wani A and Gao JX. Germline stem cell gene PIWIL2 mediates DNA repair through relaxation of chromatin. PLoS One 2011; 6: e27154.

[15] Lee JH, Jung C, Javadian-Elyaderani P, Schweyer S, Schütte D, Shoukier M, Karimi-Busheri F, Weinfeld M, Rasouli-Nia A, Hengstler JG, Mantilla A, Soleimanpour-Lichaei HR, Engel W, Robson CN and Nayernia K. Pathways of proliferation and antiapoptosis driven in breast cancer stem cells by stem cell protein piwil2. Cancer Res 2010; 70: 4569-4579.

[16] Zhang D, Wu X, Liu X, Cai C, Zeng G, Rohozinski J, Zhang Y, Wei G and He D. Piwil2-transfected human fibroblasts are cancer stem cell-like and genetically unstable. Oncotarget 2017; 8: 12259-12271.

[17] Wang YY, Zhang CY, Ma YQ, He ZX, Zhe H and Zhou SF. Therapeutic effects of C-28 methyl ester of 2-cyano-3,12-dioxoolean-1,9-dien-28-oic acid (CDDO-Me; bardoxolone methyl) on radiation-induced lung inflammation and fibrosis in mice. Drug Des Devel Ther 2015; 9: 3163-3178.

[18] Cho YJ, Yi CO, Jeon BT, Jeong YY, Kang GM, Lee JE, Roh GS and Lee JD. Curcumin attenuates radiation-induced inflammation and fibrosis in rat lungs. Korean J Physiol Pharmacol 2013; 17: 267-274.

[19] Kulkarni AA, Thatcher TH, Hsiao HM, Olsen KC, Kottmann RM, Morrissette J, Wright TW, Phipps RP and Sime PJ. The triterpenoid CDDO-Me inhibits bleomycin-induced lung inflammation and fibrosis. PLoS One 2013; 8: e63798.

[20] Tanaka A, Tanizawa H, Sriswasdi S, Iwasaki O, Chatterjee AG, Speicher DW, Levin HL, Noguchi E and Noma K. Epigenetic regulation of condensin-mediated genome organization during the cell cycle and upon DNA damage through histone H3 lysine 56 acetylation. Mol Cell 2012; 48: 532-546.

[21] Ahn WS and Antoniewicz MR. Metabolic flux analysis of CHO cells at growth and non-growth

phases using isotopic tracers and mass spectrometry. Metab Eng 2011; 13: 598-609.
[22] Vujaskovic Z and Groen HJ. TGF-beta, radiation-induced pulmonary injury and lung cancer. Int J Radiat Biol 2000; 76: 511-516.
[23] Zhang K, Lu Y, Yang P, Li C, Sun H, Tao D, Liu Y, Zhang S and Ma Y. HILI inhibits TGF-beta signaling by interacting with Hsp90 and promoting TbetaR degradation. PLoS One 2012; 7: e41973.
[24] Zhao H, Dennery PA and Yao H. Metabolic reprogramming in the pathogenesis of chronic lung diseases, including BPD, COPD, and pulmonary fibrosis. Am J Physiol Lung Cell Mol Physiol 2018; 314: L544-L554.
[25] Jiang S, Zhao L, Lu Y, Wang M, Chen Y, Tao D, Liu Y, Sun H, Zhang S and Ma Y. Piwil2 inhibits keratin 8 degradation through promoting p38-induced phosphorylation to resist Fas-mediated apoptosis. Mol Cell Biol 2014; 34: 3928-3938.
[26] Carrieri C, Comazzetto S, Grover A, Morgan M, Buness A, Nerlov C and O'Carroll D. A transit-amplifying population underpins the efficient regenerative capacity of the testis. J Exp Med 2017; 214: 1631-1641.
[27] Vander Heiden MG and DeBerardinis RJ. Understanding the intersections between metabolism and cancer biology. Cell 2017; 168: 657-669.
[28] Yin J, Ren W, Huang X, Deng J, Li T and Yin Y. Potential mechanisms connecting purine metabolism and cancer therapy. Front Immunol 2018; 9: 1697.
[29] Moon HG, Tae YM, Kim YS, Gyu Jeon S, Oh SY, Song Gho Y, Zhu Z and Kim YK. Conversion of Th17-type into Th2-type inflammation by acetyl salicylic acid via the adenosine and uric acid pathway in the lung. Allergy 2010; 65: 1093-1103.
[30] Yu M, Cui FX, Jia HM, Zhou C, Yang Y, Zhang HW, Ding G and Zou ZM. Aberrant purine metabolism in allergic asthma revealed by plasma metabolomics. J Pharm Biomed Anal 2016; 120: 181-189.
[31] Wang Y, Liu Y, Cao Q, Shi X, Lu H, Gao S and Yang R. Metabolomic analysis for the protective effects of mangiferin on sepsis-induced lung injury in mice. Biomed Chromatogr 2018; 32: e4208.
[32] Ian VP, Schneider F, Novelli EM, Kelley EE, Shiva S, Gladwin MT, Jackson EK and Tofovic SP. Experimental intravascular hemolysis induces hemodynamic and pathological pulmonary hypertension: association with accelerated purine metabolism. Pulm Circ 2018; 8: 2045894018791557.

Table S1. Primers Used in Study

Target	Forward	Reverse
Nrf2	CGGTATGCAACAGGACATTG	TTGGCTTCTGGACTTGGAAC
POLN	TTGACGCTGAAGGGAGGGAGT	TGAATCTGGCTGATGCCCTACA
PIWIL2	AAGGTCCTAAATAGATGTCCACG	GGGTATGCACATTGGGTTTC
CDHR3	CTAGGTTTGGGACGCAGGG	GGTCACCAACGAGGGATAGAG
GSTA4	CTCAAGATGTCCCACTGAGATG	TAAGGGTGTTAAGCAGGCAAA
CYSLTR2	GCCATGATTGTGGATCAGATAGG	CTACGTGTGAGCTTTCCCCAG
LILRB1	TAGACCAATGGAACAGAATAGAA	CCAGTTTCAATTGTCTGCATAT
SNX16	CCTTTTCTCACTCTTAGTCGGGC	CTTGGGCTTGGAAAGTTGGAG
COL6A1	GGATTGGAAACTACCGAAAGATG	TGAAAACCAGCGTGTCACCC
USP17L2	AGGTTATCCCTGGAAGGTCTG	GGCAGCTACCGTCATCCTC
IMPDH1	GTCTGCATCCCCCAACCAAAG	ACTGCTGCAGGCCGGCTAC
IMPDH2	GCTCCTGTGCCTGATGGAAT	CGGGCTCCTCCCCAAAATAA
β-actin	CTCCATCCTGGCCTCGCTGT	GCTGTCACCTTCACCGTTCC